SUPPLEMENTARY FIGURES

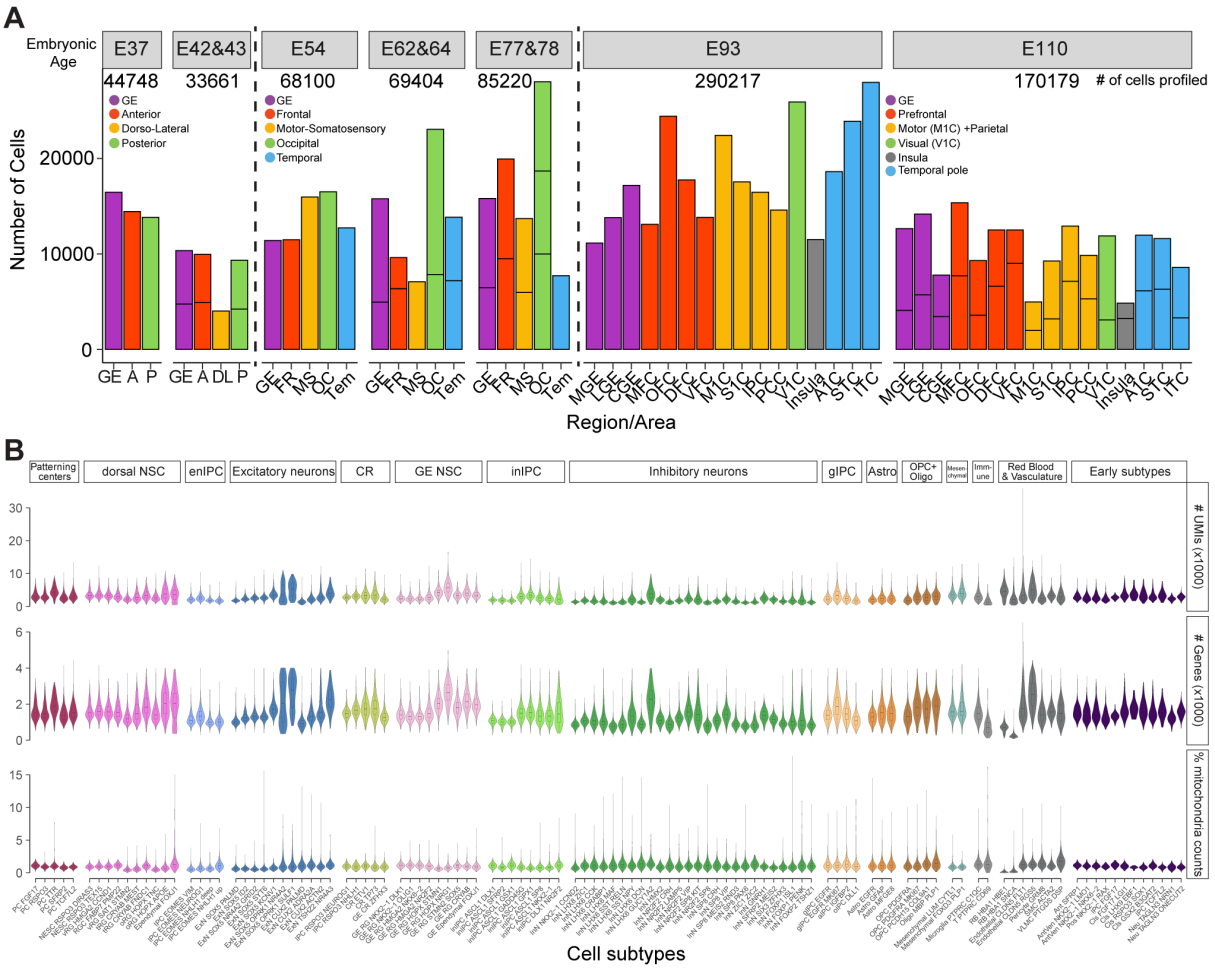

Fig. S1. Quality overview of the fetal macaque telencephalic scRNA-seq data (**A**) Bar plot displaying the sample size. Each segment represents a biological replicate. Number of cells at each age passing quality control is indicated. At earliest phases (E37 to E78), ganglionic eminence (GE), anterior (A)/frontal (FR), dorso-lateral (DL)/putative motor-somatosensory (MS), posterior (P, temporo-occipital)/occipital (OC) and putative temporal telencephalic regions were recognized. At the latest stages (E93 and E110), more refined areas could be collected: three from GE (medial: MGE; lateral: LGE; caudal: CGE) and up to 13 from prospective prefrontal (medial: MFC; orbital: OFC; dorsolateral: DFC/dlPFC; ventrolateral: VFC), primary motor (M1C), parietal (primary somatosensory: S1C; inferior parietal: IPC; posterior cingulate: PCC), occipital (primary visual: V1C), insula (Ins), temporal (primary auditory: A1C; superior: STC; inferior: ITC) cortical wall. (**B**) Violin plot showing quality metrics of the identified cell subtypes.

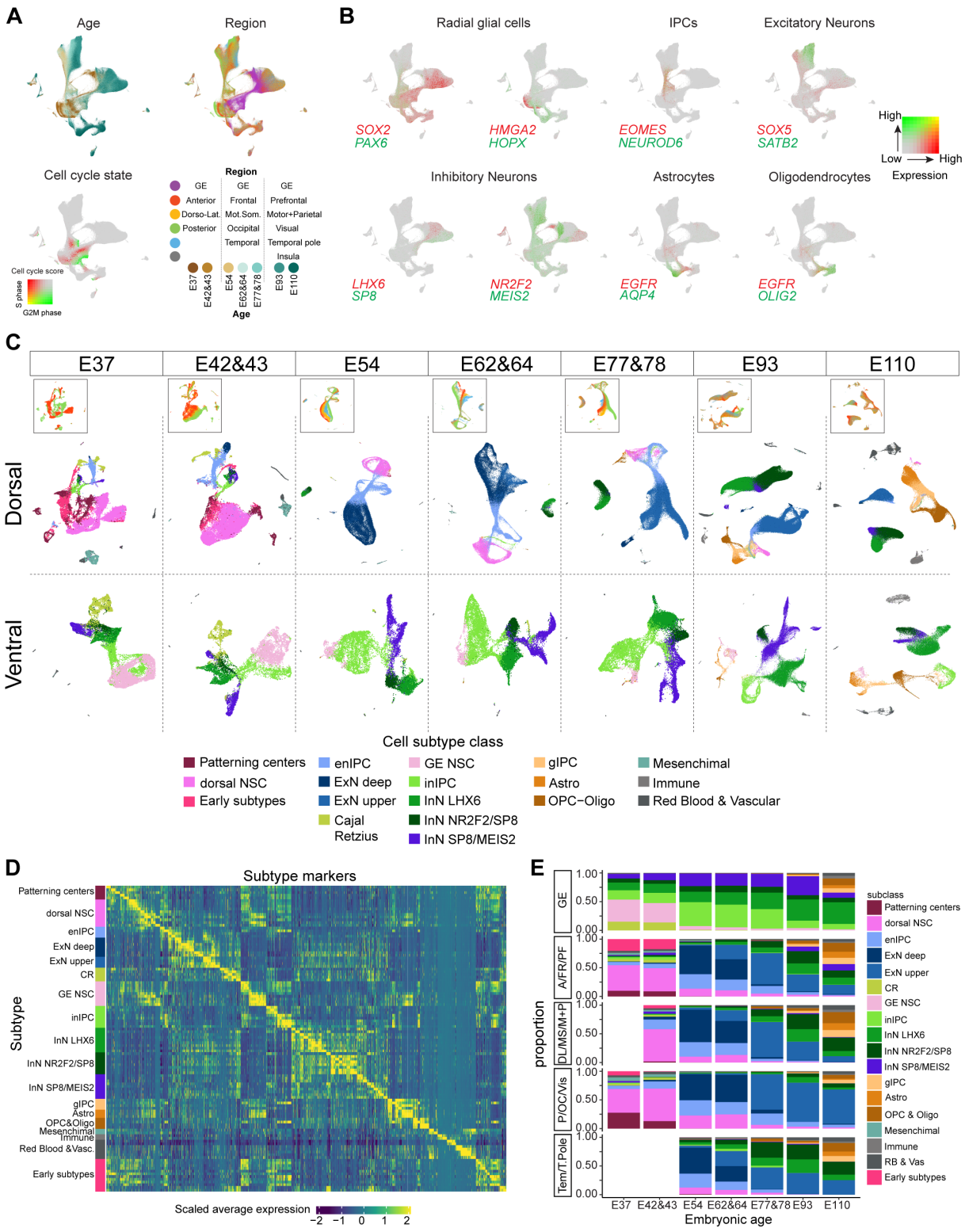

Fig. S2. Spatiotemporal transcriptomic overview of cell subtypes (**A**) Age, region and cell cycle score distribution on the UMAP layout. (**B**) Expression of the major class markers on the UMAP. (**C**)

Spatiotemporal dynamics of different major dorsal and ventral cell subtypes. Regions (insets) as indicated in the legend in A. (**D**) Top marker genes distinguishing different cell subtypes. **(E)** Proportion of the main cell subtypes across regions and age. Regions across the embryonic ages follow the scheme in A. NSC: neural stem cells; IPC: intermediate precursors cells; enIPC: excitatory neuron IPC; ExN: excitatory neurons; CR: Cajal-Retzius neurons; inIPC: inhibitory neuron IPC; InN: inhibitory neurons; gIPC: glial IPC; aIPC: astrocyte IPC; Astro: astrocytes; Oligo: oligodendrocyte; OPC: oligodendrocyte precursor cells; Mes: mesenchymal cells; Imm: immune cells; RB and Vas: red blood lineage and vascular cells.

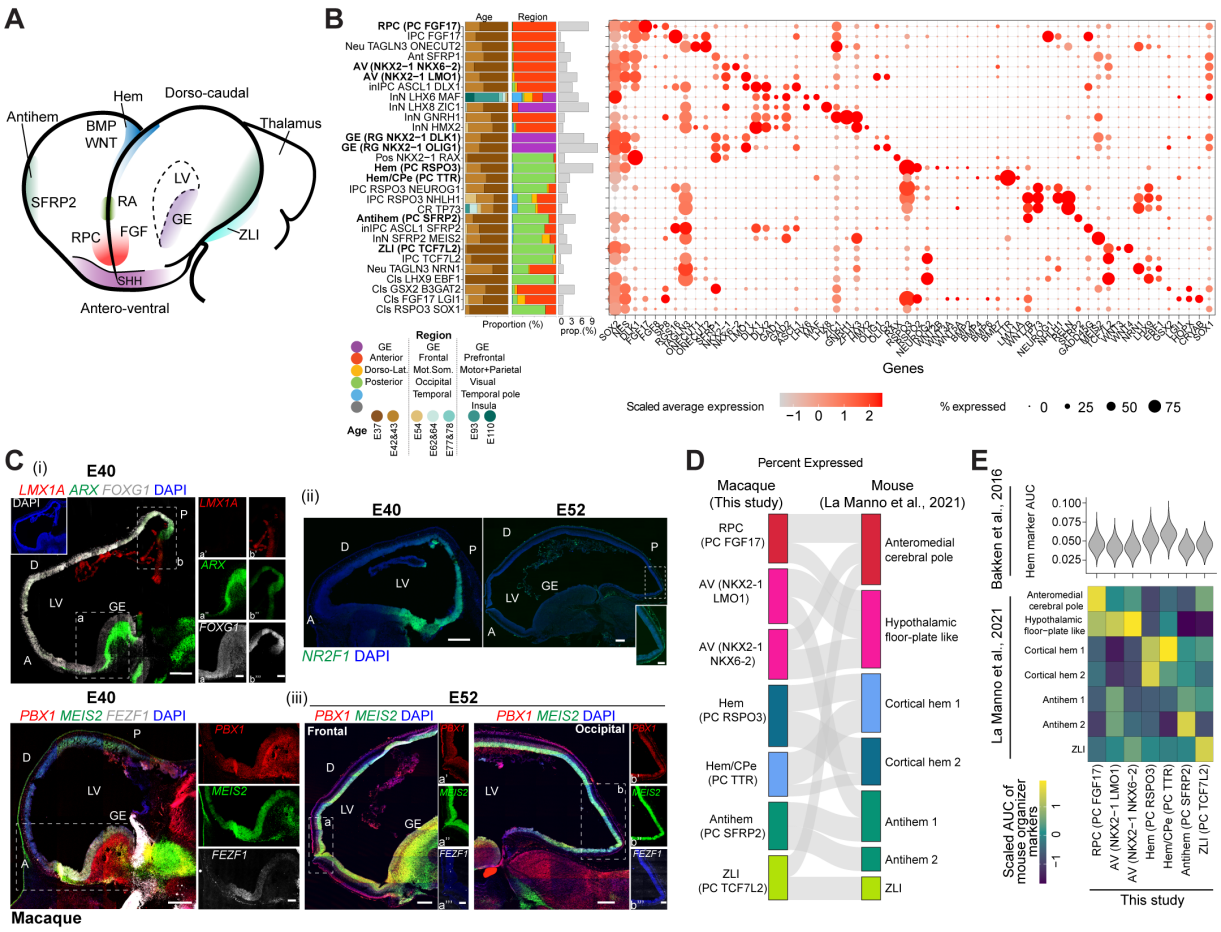

Fig. S3. Molecular characterization of the monkey putative telencephalic organizer domains (A) Schema illustrating the mammalian early developing telencephalon and the patterning centers (or organizers) secreting signaling molecules, adapted from (*3*). The antero-ventral (AV) domain secreting SHH is adjacent to the anterior neural ridge/rostral patterning center (RPC) secreting FGFs (*20, 21*); cortical hem is in the posterior domain secreting WNTs and BMPs (*22, 23*); zona limitans intrathalamica (ZLI) is caudal-ventral, between posterior telencephalon and thalamus (*24*); antihem is at the dorsal-ventral pallium boundary, secreting WNT antagonist *SFRP2* (*53*); the ganglionic eminence (GE) is in the ventral telencephalon. Notice retinoic acid (RA) signaling from the anterior region (*31*). (**B**) Left bar plots: age, region composition and cluster proportions of the early cell subtypes. Region identity across the age is indicated on bottom left. Right dot plot: expression level (color gradient) and percentage of cells (dot size) expressing subtype markers. The four subtypes in the bottom (Cls LHX9 EBF1; Cls GSX2 B3GAT2; Cls FGF17 LGI1; Cls RSPO3 SOX1) were small in size and their identities were left as unknown. (**C**) Expression of the patterning genes *LMX1A*, *ARX*, *FOXG1* (i), *NR2F1* (ii) and *PBX1*,

MEIS2, FEZF1 (iii), detected by RNAscope in monkey E40 and E52 sagittal brain sections. Panoramic scans are shown. Higher magnification from the dashed areas of the antero-ventral (a) and dorso-posterior (b) domains are shown (a', a'', a''' and b', b'', b'', respectively). Scale bar: 500 μm (panoramic) and 200 μm (zoom-in). FR: frontal; OC: occipital; D: dorsal; V: ventral; GE: ganglionic eminence; VZ: ventricular zone; LV: lateral ventricle. (**D**) Sankey plot illustrating the transcriptomic similarity (Pearson correlation coefficients) between macaque (this dataset) and mouse (*25*) brain organizer subtypes. A cutoff was set at the 0.8 quantile of all similarity scores to remove putative background signals. (**E**) Top: AUC score assessing the enrichment of cortical hem markers generated in (*14*). Bottom: Average AUC scores measuring the enrichment of mouse patterning center subtype markers (*25*) in macaque.

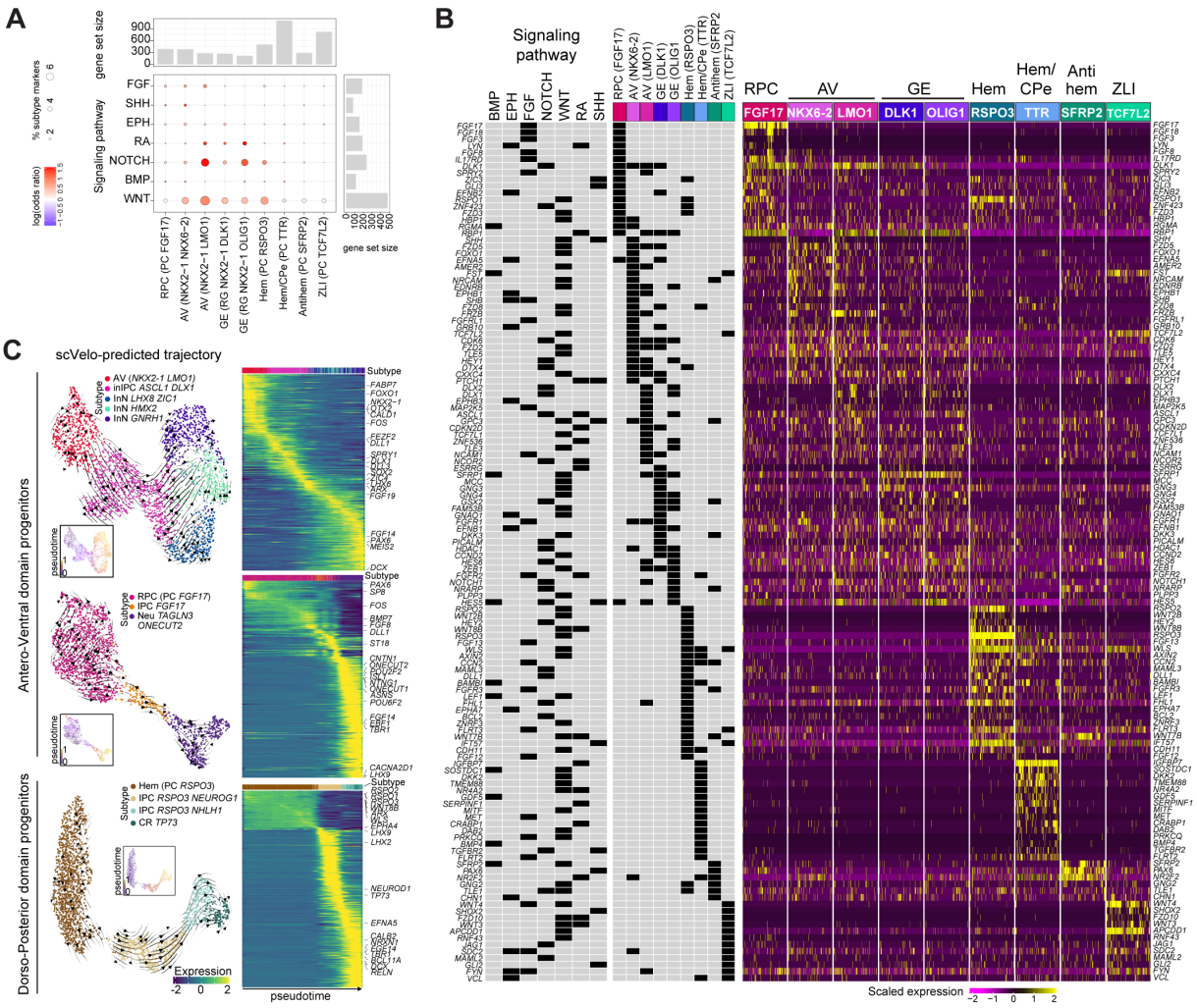

Fig. S4. Signaling pathways orchestrating telencephalic organizer functions (A) Enrichment of signaling pathway genes across the organizer domain subtypes measured by the log-transformed odds ratios of the overlapping between key signaling pathway genes and organizer domain markers. **(B)** Expression of signaling pathway genes shown as the top 100 markers of an organizer domain subtype. Signaling pathway and marker annotation are shown on the left. (**C**) Left: RNA velocity and pseudotime predicting the lineage progression of the antero-ventral *FGF17*$^{+}$ and *NKX2-1*$^{+}$ progenitors (top 2 panels) and the dorso-caudal *RSPO3*$^{+}$ progenitors (bottom panel). Right: gene expression cascades along the lineages. This analysis defines the origins of the earliest neurons generated by the telencephalic organizer centers and their transcriptional dynamics across the differentiation trajectories.

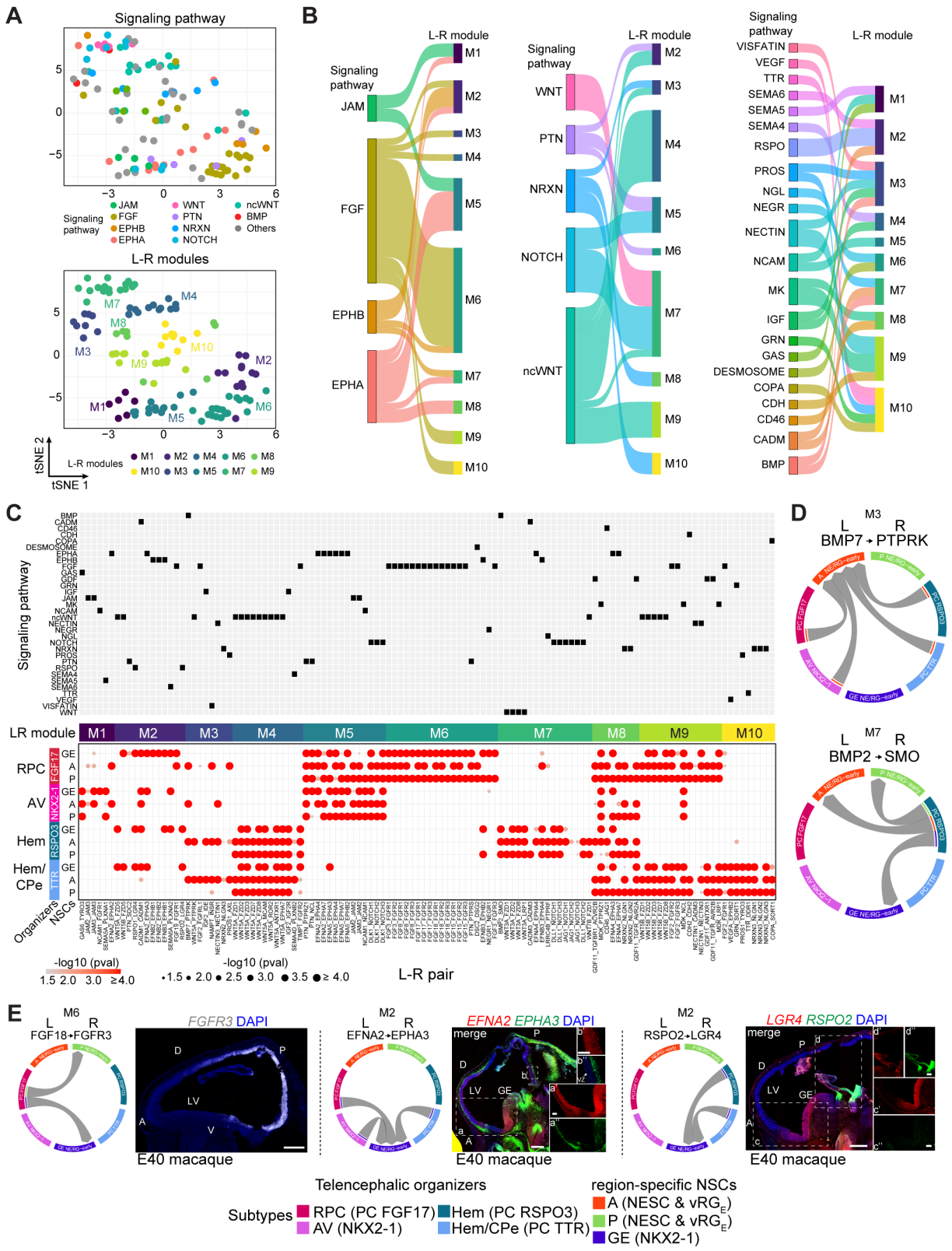

Fig. S5. Predicted cell-cell interaction between putative telencephalic organizer domains and early radial glial cells (**A**) t-distributed stochastic neighbor embedding (tSNE) plots visualizing the

signaling pathways and the co-interaction modules (M1-M10) of all the ligand-receptor (L-R) pairs (dots). Signaling pathways with low numbers of L-R pairs were annotated as “others”. (**B**) Sankey plot showing the L-R pair-mediated cell-cell interaction patterns (represented by M1-M10) of all the signaling pathways. (**C**) Top: signaling pathway annotation for each L-R pair. Bottom: interaction patterns of all the L-R pairs between organizer subtypes (RPC, AV, Hem and Hem/CPe) and E37-43 NSCs (NESCs and vRG_E) from GE, anterior (A) and posterior (P) telencehalic regions, organized by modules. (**D**) Interaction patterns of selected L-R pairs belonging to BMP signaling (*BMP7-PTPRK*, M3; *BMP2-SMO*, M7). The arrows show the interaction direction from the ligand- to the receptor-expressing cells, that is, organizer domains and A, P or GE NSCs, respectively. **(E)** Circular plots showing the interaction pattern of selected L-R pairs belonging to the indicated modules (M) related to FGF, Ephrin and WNT signaling and RNAscope of E40 macaque brain tissue sagittal sections. Panoramic scans are shown. Higher magnifications from the dashed area are shown. Scale bar: 500 μm (panoramic) and 200 μm (zoom-in).

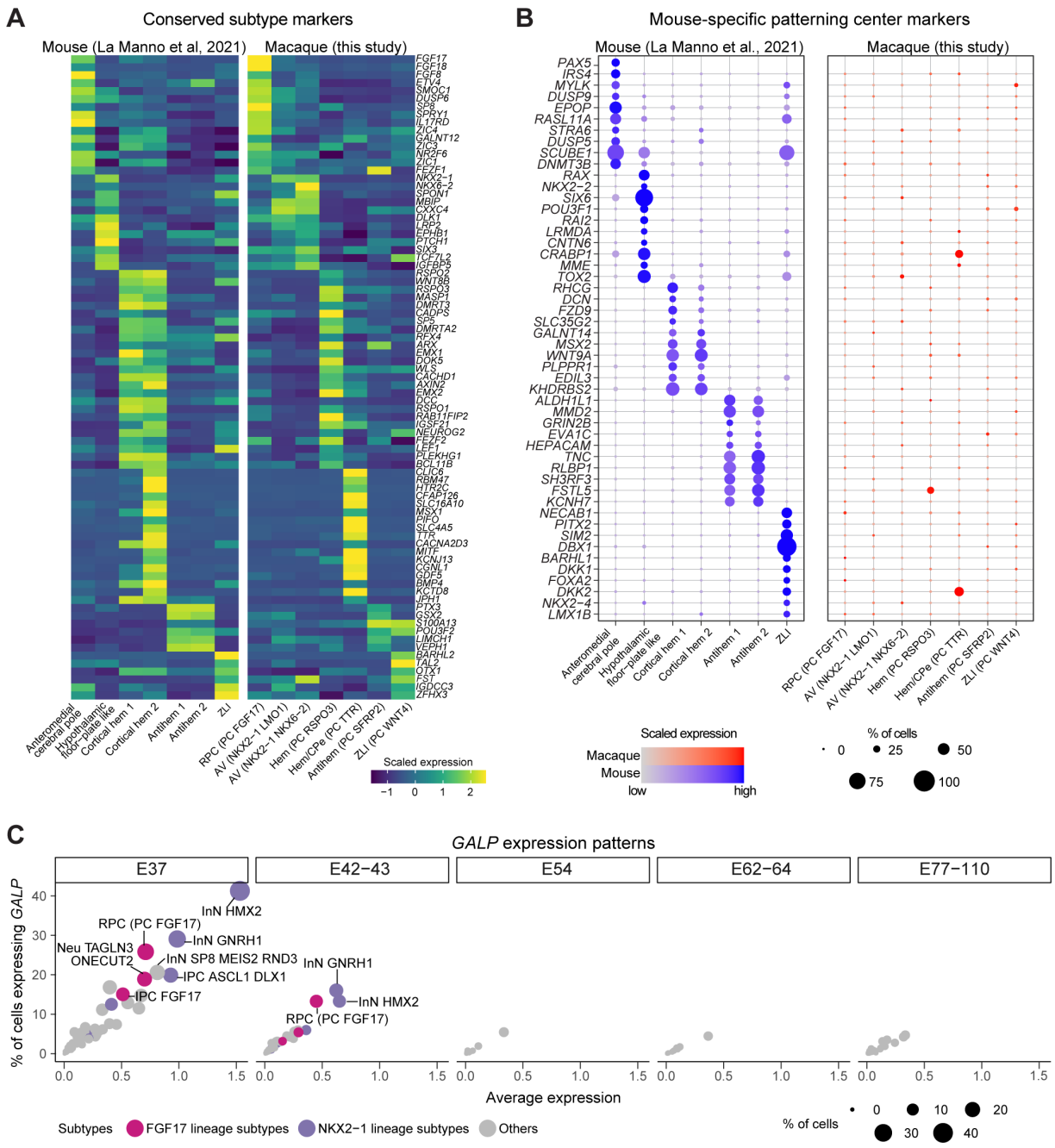

Fig. S6. Conserved and divergent transcriptomic features between mouse and macaque telencephalic organizers (A) Genes displaying conserved expression between mouse (*25*) and macaque (this study) telencephalic organizer domain subtypes, suggesting similar mechanisms of regional patterning between primate and mouse telencephalons (*4, 9*). (**B**) In contrast to the identified organizer markers specific to macaque (Fig. 3C), we also identified mouse-specific organizer markers. This plot illustrates the expression of the top 10 markers of each mouse organizer showing mouse-

enriched expression versus macaque. Dot color indicates scaled expression for each specie; dot size indicates the percentage of cells expressing a gene. (**C**) *GALP* expression across cell subtypes and developmental ages. The dot size represents percentage of cells expressing *GALP*. Top 7 cell subtypes in each age showing an expression percentage not smaller than 10% and an average log-transformed expression value not less than 0.4 of *GALP* expression are colored and labeled.

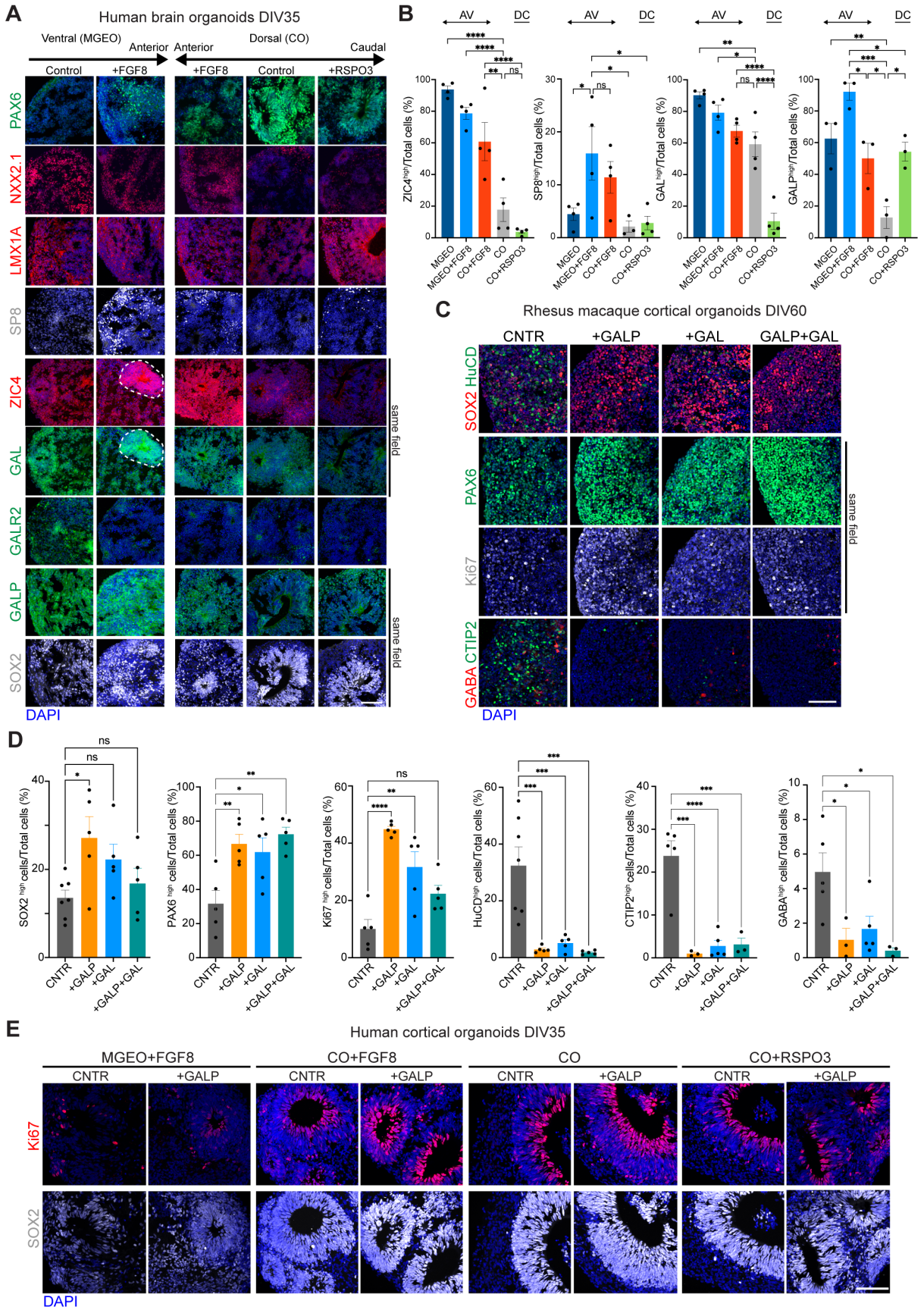
A
Human brain organoids DIV35
Ventral (MGEO)
Anterior
Anterior
Dorsal (CO)
Caudal
Control
+FGF8
+FGF8
Control
+RSPO3
PAX6
NXX2.1
LMX1A
SP8
ZIC4
GAL
GALR2
GALP
SOX2
same field
same field
DAPI
B
AV
DC
ZIC4high/Total cells (%)
SP8high/Total cells (%)
GALhigh/Total cells (%)
GALPhigh/Total cells (%)
MGEO
MGEO+FGF8
CO+FGF8
CO
CO+RSPO3
C
Rhesus macaque cortical organoids DIV60
CNTR
+GALP
+GAL
GALP+GAL
SOX2 HuCD
PAX6
Ki67
GABA CTIP2
same field
DAPI
D
SOX2 high cells/Total cells (%)
PAX6 high cells/Total cells (%)
Ki67 high cells/Total cells (%)
HuCDhigh cells/Total cells (%)
CTIP2high cells/Total cells (%)
GABAhigh cells/Total cells (%)
CNTR
+GALP
+GAL
+GALP+GAL
E
Human cortical organoids DIV35
MGEO+FGF8
CO+FGF8
CO
CO+RSPO3
CNTR
+GALP
Ki67
SOX2
DAPI

Fig. S7. The function of GALP on NSCs evaluated using brain organoids (A and B) To recapitulate early events of brain development in vitro (*92, 93*), cortical (hCO) and medial ganglionic eminence (hMGEO) organoids were generated from human induced pluripotent stem cells (iPSCs) and differentiated up to day in vitro (DIV) 35. Human COs were exposed to dorso-caudal or antero-ventral patterning signals, that is RSPO3 or FGF8, respectively, or to control conditions. Human MGEO were exposed to FGF8 or control conditions. Modulation of RSPO3 and FGF8 signaling was done during the patterning phase (DIV8-21), when neuroepithelial cells form organizer states in vitro (*29*). Then, all organoids were differentiated in the same medium and analyzed at DIV35 (see materials and methods). Immunohistochemistry of standard markers, scale bar: 100 µm (A), and high-throughput image analysis showing the percentage of cells expressing the indicated proteins in the different culture conditions ± SD, One-way ANOVA, Dunnett's multiple comparisons (B). Significance is indicated. AV: antero-ventral; DC: dorso-caudal. The data shows regional molecular features of the organoids resembling the early domains of the fetal macaque telencephalon. As the expression of these regional markers was checked long after the ligand stimulation was finished, this experiment suggests that the identity of the cells was maintained after the patterning action was terminated (*93*). (**C**) The effect of exogenous GALP and GAL stimulation on proliferation of the NSCs was tested. The panel shows immunohistochemistry of the indicated genes in rhesus macaque iPSC-derived cortical organoids (rmCO), control or exposed to 30 ng/ml GALP, GAL or both ligands from DIV46 to 60, when the presence of both RG and neurons is expected. Scale bar: 100 µm. **(D)** Image analysis of at least 5 different fields showing percentage of cells expressing the indicated markers in the different conditions ± SD, One-way ANOVA, Dunnett's multiple comparison (*: $p < 0.1$; **: $p < 0.01$; ***: $p < 0.001$; ****: $p < 0.0001$; ns: not significant). The analysis shows enhanced proportion of $Ki67^+$, $SOX2^+$ and $PAX6^+$ cells and reduced $HuCD^+$, $CTIP2^+$ and $GABA^+$ neurons, indicating increased proliferation of the NSCs and compromised neuronal differentiation. (**E**) The potential role of GALP in instructing NSCs of a preferential telencephalic region was tested. Immunohistochemistry of SOX2 and Ki67 from sections of human CO or MGEO exposed or not to patterning ligands (FGF8 or RSPO3) plus/minus 30 ng/ml GALP from DIV8-21, then differentiated until DIV35 and analyzed. Scale bar: 100 µm. Quantification shown in Fig. 3F. CNTR: control.

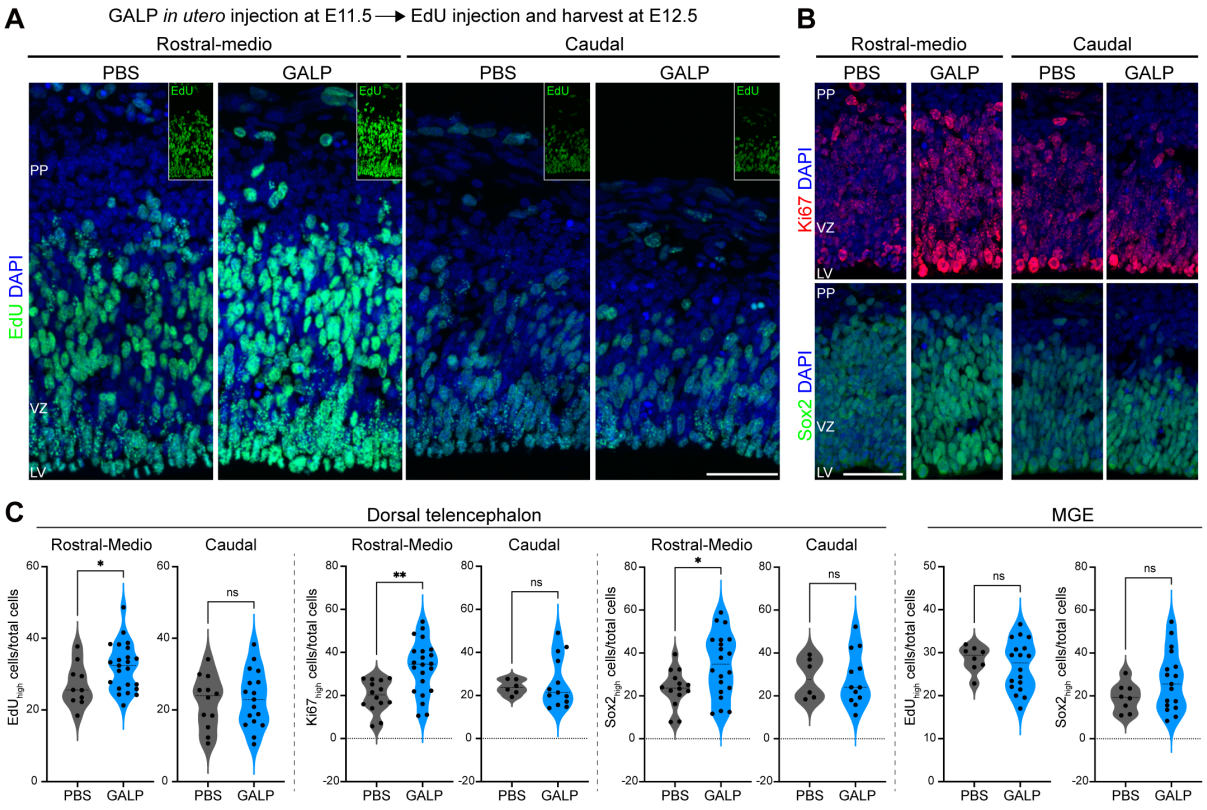

Fig. S8. Exogenous GALP increases the proliferation of frontal NSCs in embryonic mouse telencephalon (A) Intraventricular injection of PBS or 100 ng in 1µl of GALP in E11.5 mouse embryos. EdU incorporation was perfomed 2 hours before harvesting the embryos at E12.5. Immunohistochemistry for EdU in E12.5 mouse telencephalic coronal sections. Images of the dorsal telencephalon are shown. Scale bar: 50 µm. **(B)** Immunohistochemistry for Sox2 and Ki67 of the same tissue sections shown in A. Sox2 and Ki67 signals are from the same field. Scale bar: 50 µm. **(C)** Hgh-throughput quantification of the markers shown in A and B. Analysis of multiple fields (represented by each dot) imaged across sequential sections of the mouse telencephalon, from frontal to caudal dorsal regions and across sequential sections of the medial ganglionic eminence (MGE). Each dot is an average of the percentage of cells expressing high levels of the indicated markers in a field, and then plotted together for the rostral-medio versus caudal regions in the different conditions. Mann-Whitney test (*: $p < 0.1$; **: $p < 0.01$; ns: not significant). The experiment was performed using in total N=3 PBS-injected embryos and N=6 GALP-injected embryos from 2 different litters, as following: 2 controls and 4 tests littermates; 1 control and 2 tests littermates.

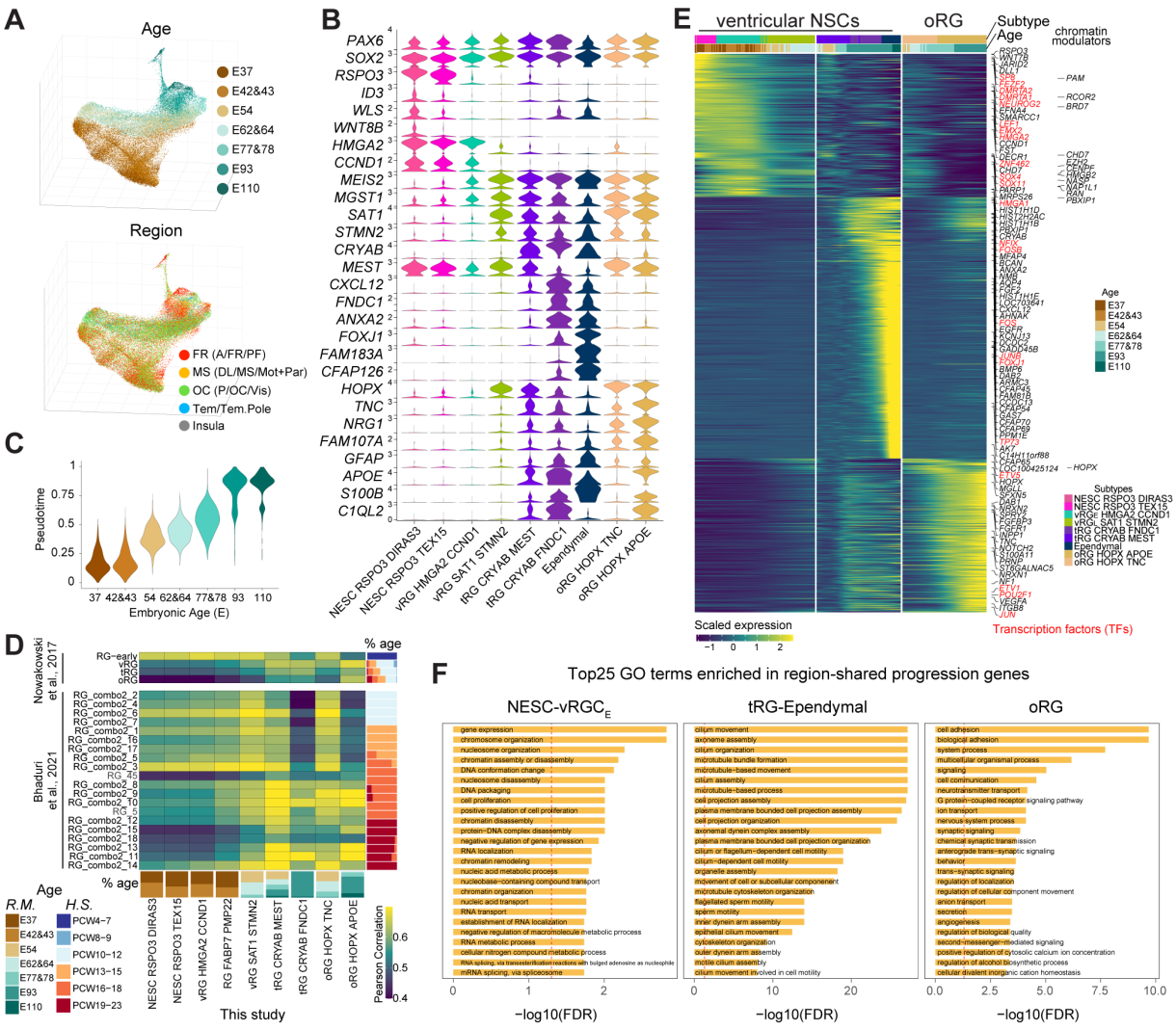

Fig. S9. Macaque cortical neural stem cell subtype characterization (A) Three-dimensional UMAP showing the age and region distribution of the NSC subtypes. The regions across the time match those in Fig. 1. (**B**) Violin plot showing expression patterns of NSC markers. (**C**) Pseudotime representing cortical NSC progression highly correlated with developmental age. (**D**) Pearson correlation measuring transcriptomic similarity between macaque (this study) and human (*15, 16*) RG subtypes, indicating higher similarity between the RG defined in (*16*) and those identified after E54 in this study. (**E**) Shared gene expression cascades across cortical regions along ventricular (or apical) NSC lineage and oRG progression. Transcription factors and non-transcription factor chromatin remodeling genes are highlighted. (**F**) Gene Ontology enrichment of the regional-shared genes in panel E. Top 25 significant terms are shown.

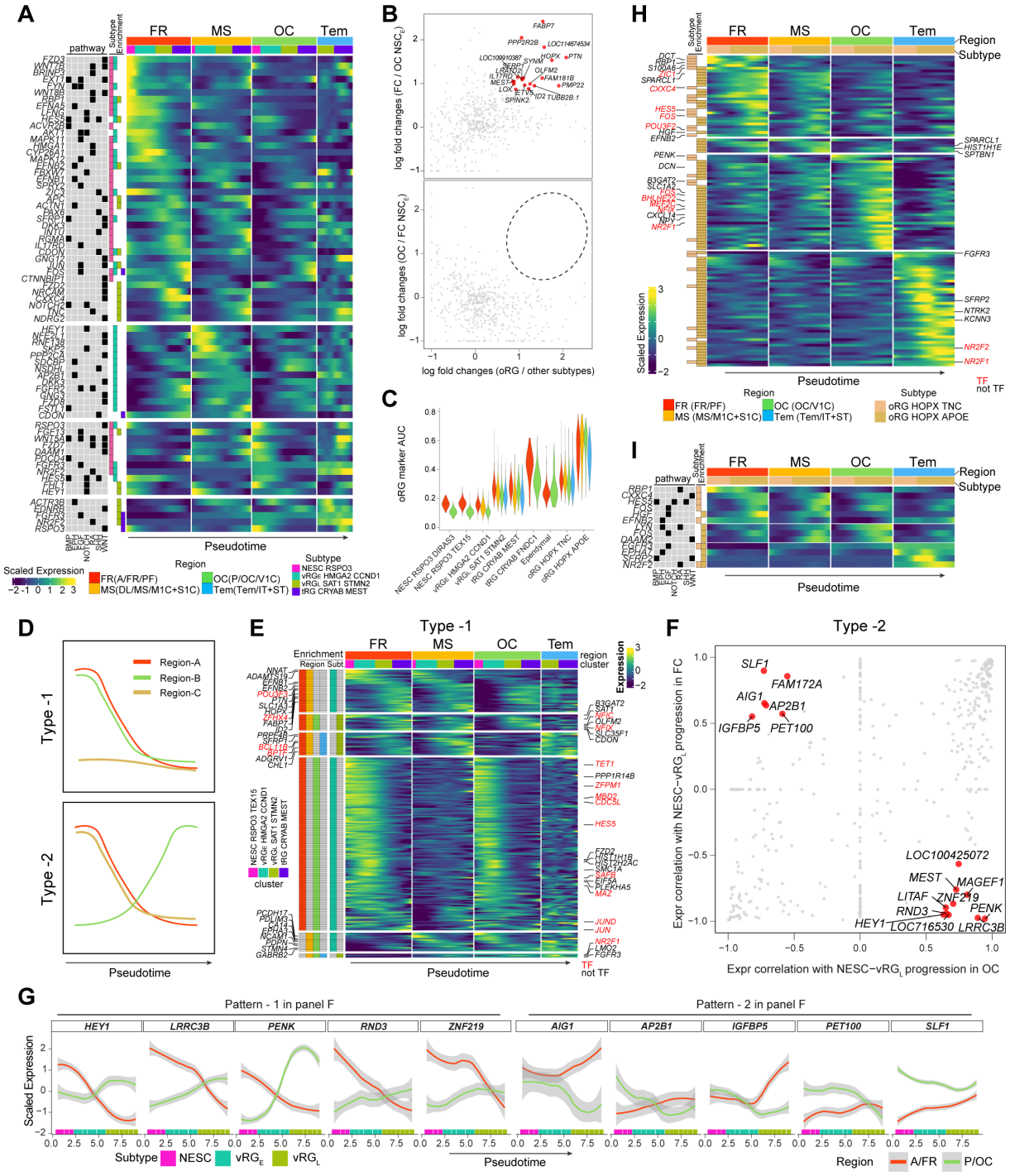

Fig. S10. Divergent transcriptomic signatures underlying neural stem cell progression across cortical regions (**A**) Expression of genes involved in the selected signaling pathways and displaying region-specificity along the progression of ventricular NSCs. The signaling pathway annotation for genes and the subtypes where they show regional expression enrichment is indicated on the left. Regions across the time match those indicated in Fig. 1. (**B**) Top: expression enrichment of regionally divergent

genes in early frontal versus occipital NSCs (y axis), and in occipital oRG versus other occipital NSCs (x axis). Genes enriched in NSCs and oRG simultaneously are shown as red dots and labeled. Bottom: Same as in the above panel, except the y axis shows the enrichment in early occipital versus frontal NSCs. Unlike frontal early NSCs and oRG, no genes were found to be enriched in early occipital NSCs and oRG simultaneously. (**C**) AUC scores assessing the enrichment of the occipital oRG subtype markers across all telencephalic regions collected and NSC subtypes. (**D**) Diagrams illustrating two models of region-specific genes employed by more than one region. (**E**) Expression cascades of genes enriched in multiple, but not all regions displaying similar expression dynamics (Type-1 genes in D). Subtype and regions employing same genes are indicated on the left of the heatmap. The regions and cell subtyes considered are the same as in A on the top. Selected genes annotated as transcription factor are colored in red (**F**) Gene expression correlation of NSC progression in the frontal versus occipital region. Genes showing expression patterns positively correlated with occipital VZ NSC progression but negatively correlated with frontal VZ NSC progression, or viceversa, were highlighted and labeled (Type-2 genes in D). (**G**) Expression patterns of some representative genes highlighted in panel F. (**H**) Region-specific gene expression cascades along the progression of oRG. Cell subtype and region information are shown on the top and in the legend. The regions follow the nomenclature across developmental time shown in Fig. 1. (**I**) Same as in H, genes involved in the selected signaling pathways are shown.

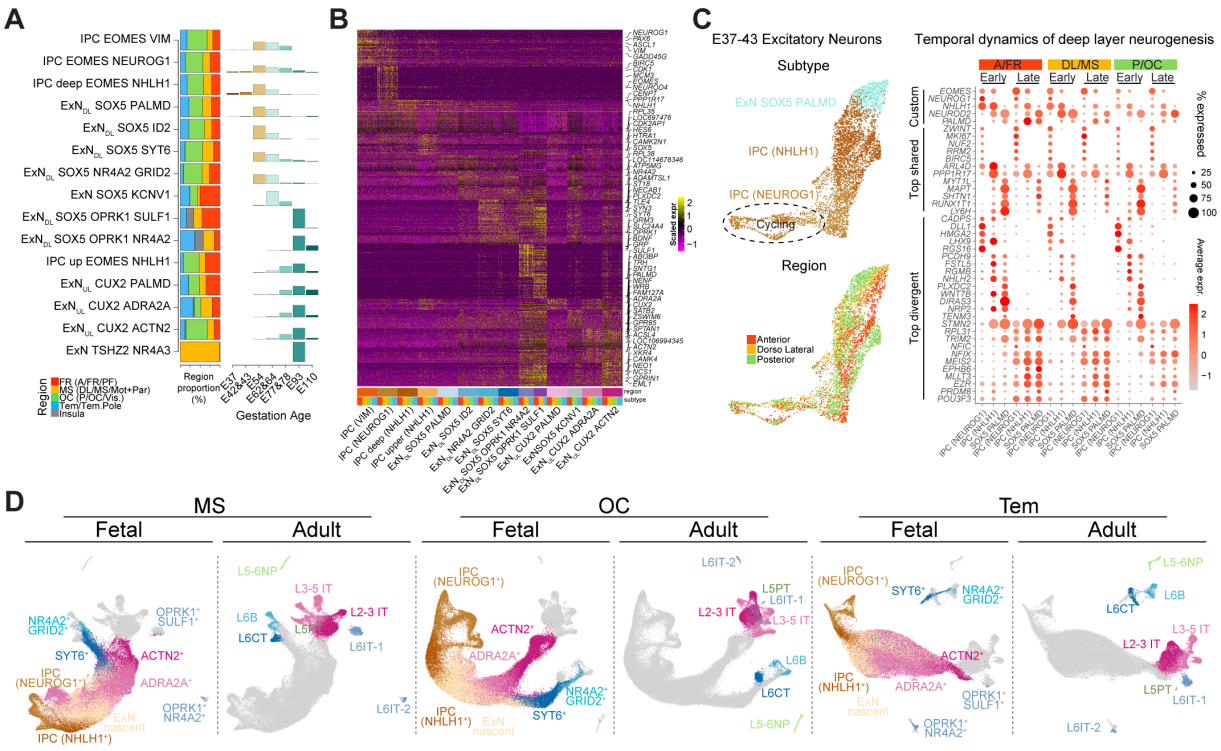

Fig. S11. Characterization of excitatory neuron differentiation and maturation (A) Age and region proportion of each cell subtype in the excitatory neuron lineage. Notice multiple subtypes of IPCs, deep and upper layer cortical neurons with different appearance across the time. The legend indicates the regions across the time from each domain, as indicated in Fig. 1. (**B**) Expression of regionally-shared markers of IPC and excitatory neuron subtypes. Region information are indicated with colors as in A, on the bottom of the heatmap. Notice that the clusters ExN TSHZ2/NR4A3 and SOX5/KCNV1 were small in size and not identified as evident deep or upper layer neurons. (**C**) Left: Early emergence (E37-43) of deep layer excitatory neurons. Right: Expression of some canonical marker genes (custom), top subtype markers shared between E37-43 and E54-64 deep layer excitatory neurons (top shared), top subtype markers specific to E37-43 or E54-64 deep layer excitatory neurons (top divergent). This early-wave of excitatory neurons share signatures with the deep layer excitatory neurons generated at E54-64, although the neurons of both phases also exhibit many divergent transcriptomic changes. The analysis denotes the identity of the early deep layer excitatory neurons and the molecular dynamics underlying their maturation. (**D**) Pairwise transcriptomic integration between the fetal excitatory neuron lineage of a given region analyzed in this study and the excitatory neurons from the adult macaque dorsolateral prefrontal cortex (*30*).

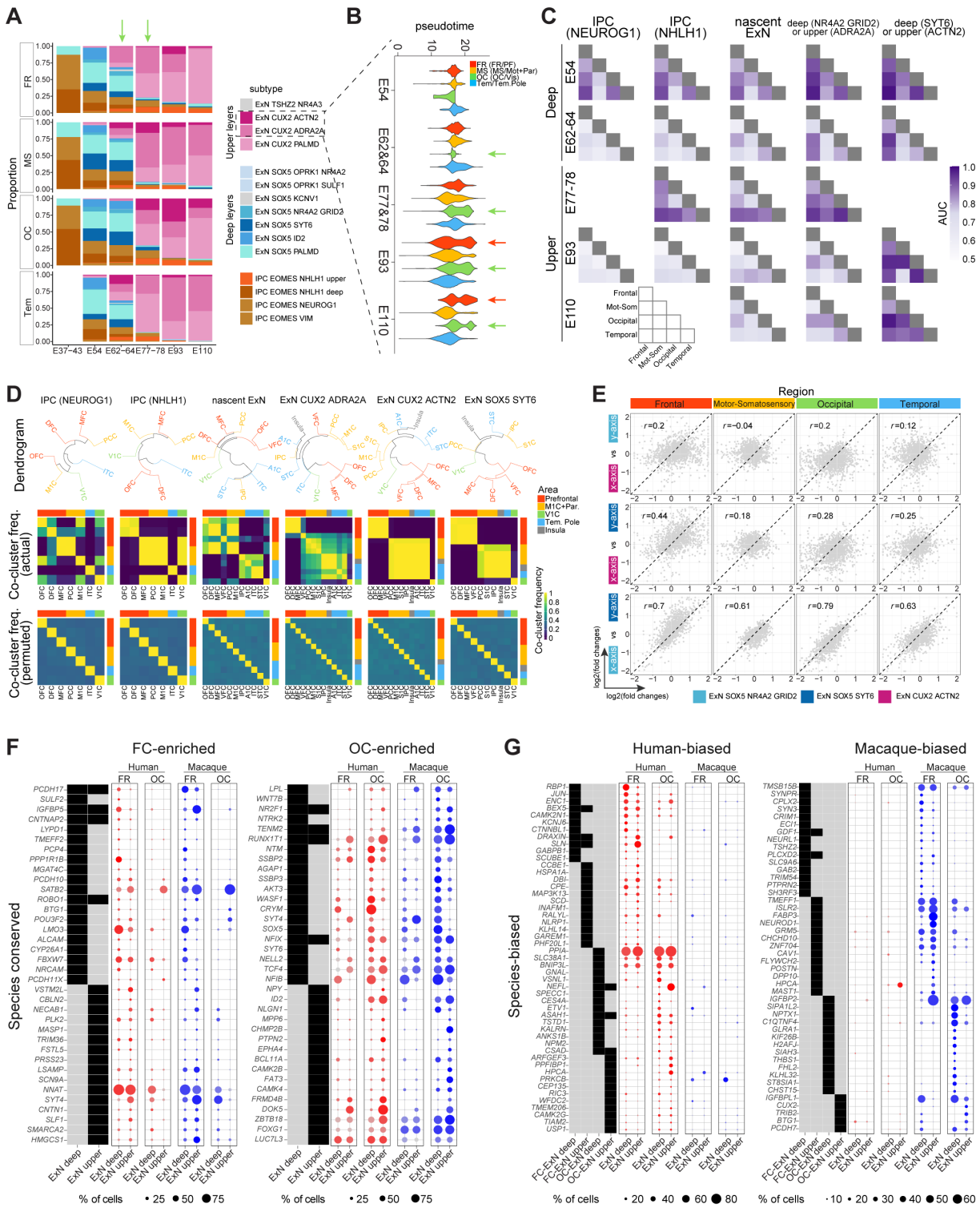

Fig. S12. Molecular programs underlying neuronal diversification across cortical regions and species (A-B) Composition of IPC and excitatory neuron subtypes in each cortical region across the timepoints. Upper layer excitatory neurons emerge around E62-64 in prefrontal, motor-somatosensory

and temporal, but not in the occipital regions (arrows on the top) (A). However, these neurons mature faster in the occipital cortex at E77-78, as depicted by the pseudotime scores. Their maturation state remain higher in prefrontal and occipital regions at E93-E110 (B). **(C)** Increasing transcriptomic divergence, represented by AUC scores calculated by Augur (see material and methods), across cortical regions in the subtypes along the differentiation and maturation lineage of the excitatory neurons. Subtypes without sufficient cells in all cortical regions were not included. **(D)** Top: Hierarchial clustering of cortical areas for each cell subtype using highly variable genes. Middle: Co-clustering frequencies of pairwise areas for each subtype using bootstrap replicates of the highly variable genes. Bottom: Co-clustering frequencies of pairwise areas using permuted data. Although divergence emerge at IPC cells, these differences were not sufficient to distinguish areas with a pattern resembling their anatomical organizations, which does not occur until the generation of more mature excitatory neuron subtypes (ExN *CUX2 ACTN2* and ExN *SOX5 SYT6*). These late excitatory neurons from different cortical areas were hierarchically distinguished into three major groups: prefrontal, motor-somatosensory and temporal, and visual region. When for certain cell types there were not sufficient cells in the areas, they were not included in the analysis. The order of the areas in the plot is based on both the overall clustering pattern and the anatomical layout of areas. (**E**) Correlation of regional enrichment between deep and upper excitatory neuron subtypes for genes divergently expressed across regions, using the peak stages of deep (E54-64) and upper layer (E93-110) neurogenesis. The regional enrichment is represented by the log fold changes of average expression in a given region versus the background regions. The Pearson correlation coefficients are listed on the top left of each panel. Notice high Pearson correlation coefficients between the late deep layer excitatory neuron subtypes, indicating overlapping of the region-specific signatures (bottom panels). The same analysis was not performed for the upper layer neurons because only one late-phase differentiated subtype was identified. Notice low correlation between deep and upper layer excitatory neuron subtypes. **(F-G)** Cross-species comparative analysis of the development of cortical regions in primates (see materials and methods). Comparison of scRNA-seq dataset of frontal and occipital human developing cortical regions at GW18-19 (*16*) with corresponding regions in macaques at the matching developmental phase E77-78 (*13*). Top shared (F) and species-biased regional (G) signatures are visualized.

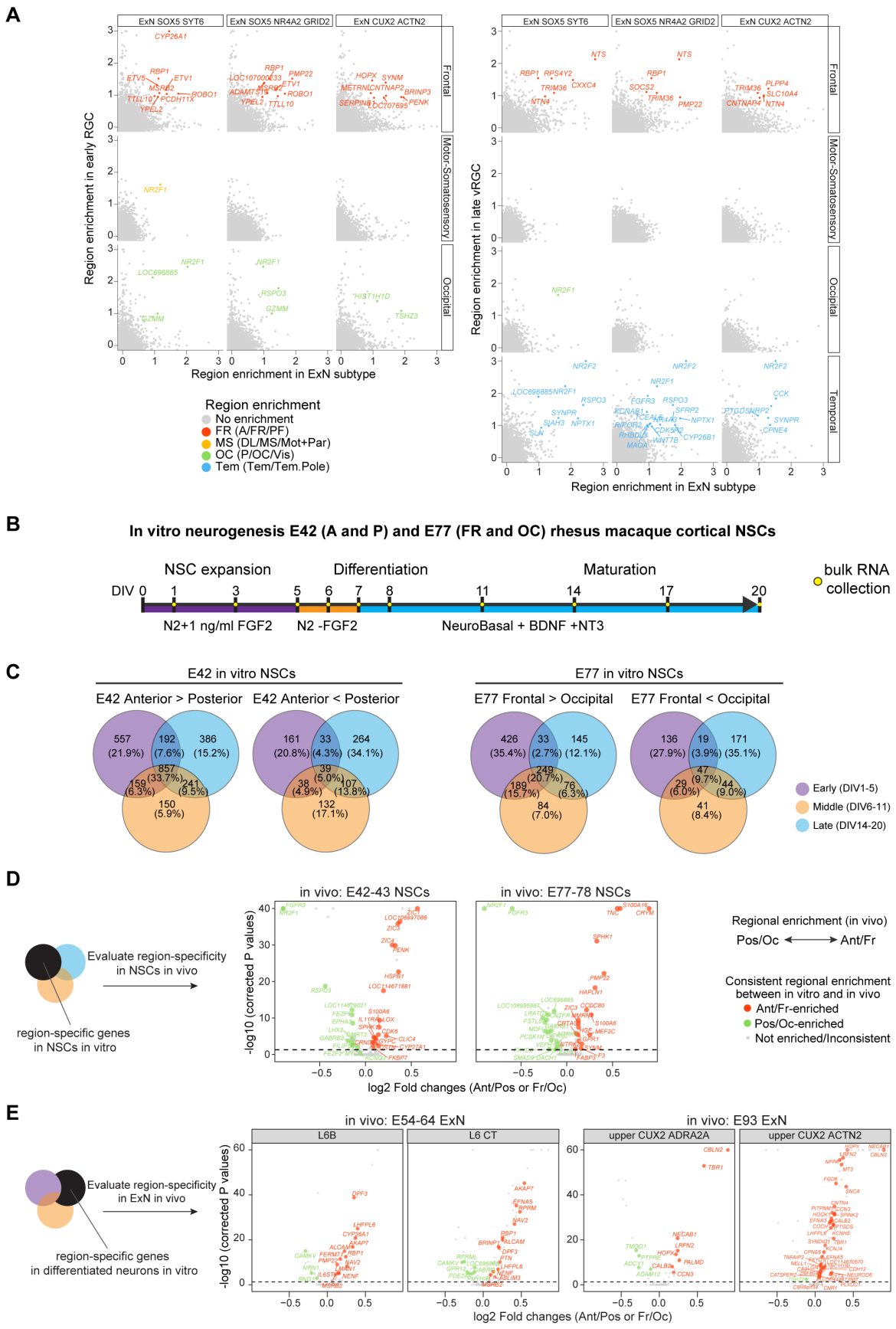
A
ExN SOX5 SYT6
ExN SOX5 NR4A2 GRID2
ExN CUX2 ACTN2
Frontal
Motor-Somatosensory
Occipital
Temporal
Region enrichment in early RGC
Region enrichment in late vRGC
Region enrichment in ExN subtype
Region enrichment
No enrichment
FR (A/FR/PF)
MS (DL/MS/Mot+Par)
OC (P/OC/Vis)
Tem (Tem/Tem.Pole)
B
In vitro neurogenesis E42 (A and P) and E77 (FR and OC) rhesus macaque cortical NSCs
NSC expansion
Differentiation
Maturation
DIV 0 1 3 5 6 7 8 11 14 17 20
bulk RNA collection
N2+1 ng/ml FGF2
N2 -FGF2
NeuroBasal + BDNF +NT3
C
E42 in vitro NSCs
E42 Anterior > Posterior
E42 Anterior < Posterior
E77 in vitro NSCs
E77 Frontal > Occipital
E77 Frontal < Occipital
557 (21.9%)
192 (7.6%)
386 (15.2%)
857 (33.7%)
159 (6.3%)
241 (9.5%)
150 (5.9%)
161 (20.8%)
33 (4.3%)
264 (34.1%)
39 (5.0%)
38 (4.9%)
107 (13.8%)
132 (17.1%)
426 (35.4%)
33 (2.7%)
145 (12.1%)
249 (20.7%)
189 (15.7%)
76 (6.3%)
84 (7.0%)
136 (27.9%)
19 (3.9%)
171 (35.1%)
47 (9.7%)
29 (6.0%)
44 (9.0%)
41 (8.4%)
Early (DIV1-5)
Middle (DIV6-11)
Late (DIV14-20)
D
Evaluate region-specificity in NSCs in vivo
region-specific genes in NSCs in vitro
in vivo: E42-43 NSCs
in vivo: E77-78 NSCs
-log10 (corrected P values)
log2 Fold changes (Ant/Pos or Fr/Oc)
Regional enrichment (in vivo)
Pos/Oc ⟷ Ant/Fr
Consistent regional enrichment between in vitro and in vivo
Ant/Fr-enriched
Pos/Oc-enriched
Not enriched/Inconsistent
E
Evaluate region-specificity in ExN in vivo
region-specific genes in differentiated neurons in vitro
in vivo: E54-64 ExN
in vivo: E93 ExN
L6B
L6 CT
upper CUX2 ADRA2A
upper CUX2 ACTN2
-log10 (corrected P values)
log2 Fold changes (Ant/Pos or Fr/Oc)

Fig. S13. Association between NSC protomap and region specificity of the post-mitotic excitatory neurons (**A**) Dotplot showing the overlap of region-specific signatures between early or late NSC subtypes and excitatory neuron subtypes. Shared region-specific genes are colored by regions and labeled. Regions across time match those in Fig. 1. (**B**) Experimental design. Monkey fetal primary NSCs were isolated from anterior and posterior telencephalic regions at E42 and frontal and occipital cortical wall of E77 and expanded separately in vitro. Expanded NSCs were passaged in N2 + 1 ng/ml FGF2 (see methods), which favorites neurogenesis, as previously described (*29*). Differentiation was induced by FGF2 withdrawal at DIV5. Neurotrophins (NTs) were added from DIV7 and cells differentiated up to DIV20. Bulk RNA was collected at the indicated time points for RNAseq. (**C**) The in vitro differentiation was parcellated into three phases representing progenitors (early), newly formed (middle) and differentiated neurons (late), respectively. Regional-specific genes were identified by DESeq2 differential expression analysis for each phase and Venn diagrams were used to show phase-specific or shared regional-specific genes across the three phases. Anterior/frontal expression enrichment is indicated by “Anterior > Posterior” or “Frontal > Occipital”, and posterior/occipital enrichment is indicated by “Anterior < Posterior” or “Frontal < Occipital”. (**D**) Region-specific genes identified in the in vitro NSCs (DIV1-5) isolated from E42 and E77 were tested for their regional expression enrichment in the age-matched NSCs in vivo (E42-43 and E77-78) and visualized by the volcano plots. The x axis shows the log-transformed fold changes between the gene expression in anterior/frontal and posterior/occipital regions, with positive values representing anterior/frontal enrichment and negative values denoting posterior/occipital enrichment. The y axis shows the P values measuring the significance of the gene expression differences between regions (Wilcoxon Rank Sum test). Genes displaying consistent regional enrichment between in vivo and in vitro system were colored in red (anterior/frontal) or green (posterior/occipital). (**E**) Dot plots highlighting the region-specific genes identified in in vitro neurons which displayed consistent regional enrichment also by the in vivo excitatory neurons. Region-specific genes in the neurons in vitro (DIV14-20) and visualized also in volcano plots. The x and y axes and colors denote the same information as in (D), except that the enrichment was tested on the indicated age-matched excitatory neurons in vivo, that is E54-64 for the E42- and E93 for E77-derived in vitro neurons.

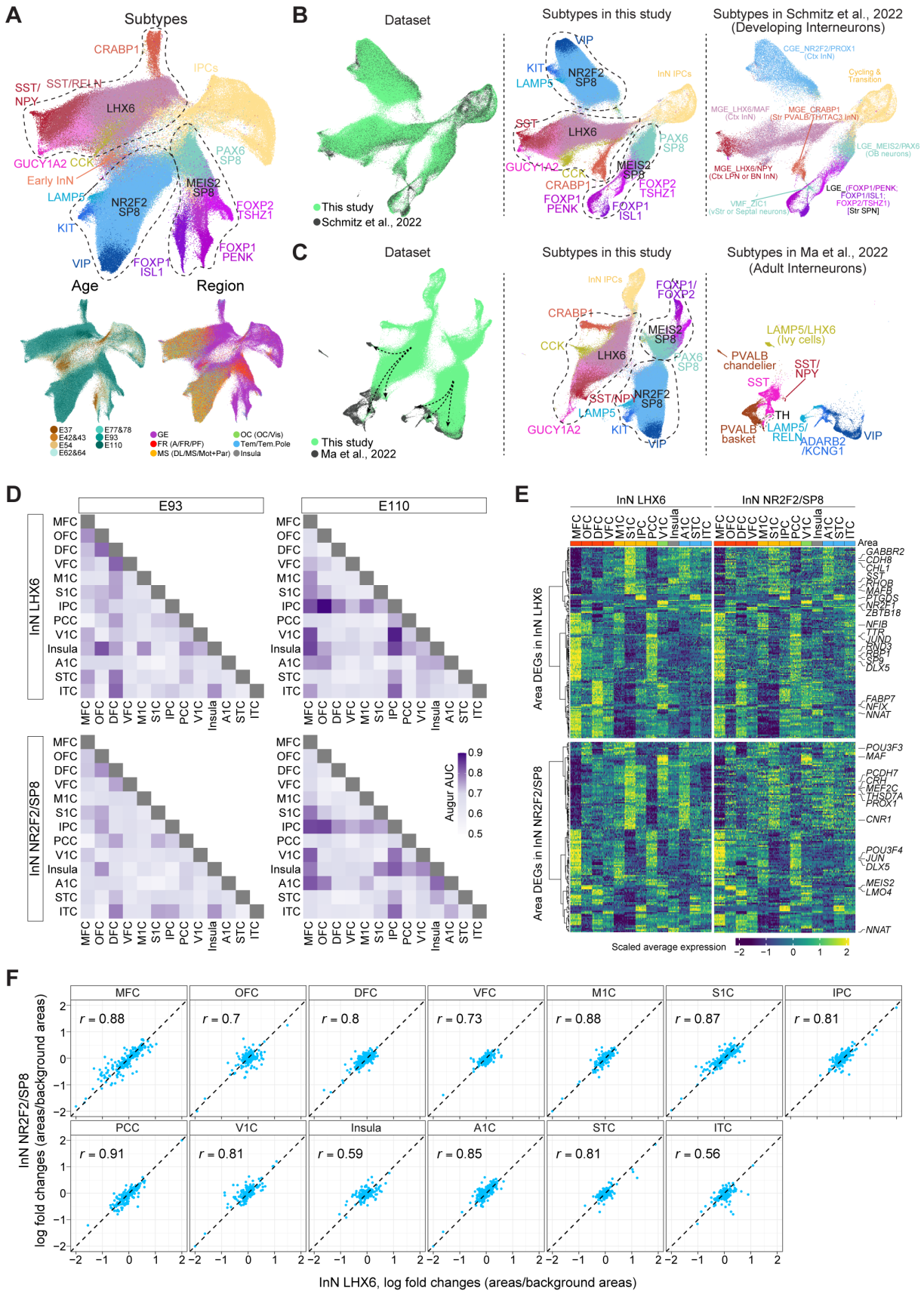
A
Subtypes
CRABP1
IPCs
SST/
NPY
SST/RELN
LHX6
PAX6
SP8
GUCY1A2
CCK
Early InN
LAMP5
NR2F2
SP8
MEIS2
SP8
FOXP2
TSHZ1
KIT
VIP
FOXP1
ISL1
FOXP1
PENK
Age
Region
E37
E42&43
E54
E62&64
E77&78
E93
E110
GE
FR (A/FR/PF)
MS (DL/MS/Mot+Par)
OC (OC/Vis)
Tem/Tem.Pole
Insula
B
Dataset
This study
Schmitz et al., 2022
Subtypes in this study
VIP
KIT
LAMP5
NR2F2
SP8
InN IPCs
SST
LHX6
PAX6
SP8
GUCY1A2
CCK
MEIS2
SP8
CRABP1
FOXP2
TSHZ1
FOXP1
PENK
FOXP1
ISL1
Subtypes in Schmitz et al., 2022
(Developing Interneurons)
CGE_NR2F2/PROX1
(Ctx InN)
Cycling &
Transition
MGE_LHX6/MAF
(Ctx InN)
MGE_CRABP1
(Str PVALB/TH/TAC3 InN)
LGE_MEIS2/PAX6
(OB neurons)
MGE_LHX6/NPY
(Ctx LPN or BN InN)
LGE_(FOXP1/PENK;
FOXP1/ISL1;
FOXP2/TSHZ1)
[Str SPN]
VMF_ZIC1
(vStr or Septal neurons)
C
Dataset
This study
Ma et al., 2022
Subtypes in this study
InN IPCs
FOXP1/
FOXP2
CRABP1
MEIS2
SP8
CCK
LHX6
PAX6
SP8
SST/NPY
NR2F2
SP8
LAMP5
GUCY1A2
KIT
VIP
Subtypes in Ma et al., 2022
(Adult Interneurons)
LAMP5/LHX6
(Ivy cells)
PVALB
chandelier
SST/
NPY
SST
TH
PVALB
basket
LAMP5/
RELN
ADARB2
/KCNG1
VIP
D
E93
E110
InN LHX6
InN NR2F2/SP8
MFC
OFC
DFC
VFC
M1C
S1C
IPC
PCC
V1C
Insula
A1C
STC
ITC
Augur AUC
0.9
0.8
0.7
0.6
0.5
E
InN LHX6
InN NR2F2/SP8
Area
Area DEGs in InN LHX6
Area DEGs in InN NR2F2/SP8
GABBR2
CDH8
CHL1
SST
RHOB
MAFB
NR2F1
ZBTB18
NFIB
TTR
JUND
RND3
RBP1
SP9
DLX5
FABP7
NFIX
NNAT
POU3F3
MAF
PCDH7
CRH
MEF2C
THSD7A
PROX1
CNR1
POU3F4
JUN
DLX5
MEIS2
LMO4
NNAT
Scaled average expression
−2
−1
0
1
2
F
MFC
OFC
DFC
VFC
M1C
S1C
IPC
PCC
V1C
Insula
A1C
STC
ITC
r = 0.88
r = 0.7
r = 0.8
r = 0.73
r = 0.88
r = 0.87
r = 0.81
r = 0.91
r = 0.81
r = 0.59
r = 0.85
r = 0.81
r = 0.56
InN NR2F2/SP8
log fold changes (areas/background areas)
InN LHX6, log fold changes (areas/background areas)

Fig. S14. Limited regional transcriptomic divergence of the cortical GABAergic inhibitory interneurons across development (A) The cortex is also populated by the GABAergic inhibitory neurons generated by the GE, migrating afterwards to the dorsal regions (*94*). Employing clustering and marker gene expression, we identified different interneuron subtypes distributed across regions and ages as shown by the UMAP. These subtypes include MGE (*LHX6*$^+$)- and CGE (*NR2F2*$^+$ and/or *SP8*$^+$)-derived cortical inhibitory neurons, the primate-specific MGE-derived (*LHX6*$^+$/*CRABP1*$^+$) inhibitory neurons and olfactory bulb neurons (*PAX6*$^+$/*SP8*$^+$), selectively abundant in the prefrontal cortex. Inhibitory subtypes were labeled with the key markers. **(B)** Transcriptomic integration with an independent developing macaque scRNA-seq dataset (*55*) confirming the subtype annotation and reaveling more interneuron heterogeneity in this study. The two datasets align well (left panel). (**C**) Transcriptomic integration between the MGE (*LHX6*$^+$)- and CGE (*NR2F2*$^+$ and/or *SP8*$^+$)-derived cortical inhibitory neurons (this study) and the adult macaque inhibitory neurons (*30*). Adult cell subtypes locate at the tips of each lineages (indicated by arrows in the left panel). The majority of the adult inhibitory neuron types matched to fetal inhibitory neuron lineages. This integration predicted putative developing trajectories from fetal to adult interneurons, including *LHX6*$^+$/*CCK*$^+$ subtype likely contributing to *LAMP5*$^+$/*LHX6*$^+$ interneurons, *SST*$^+$/*NPY*$^+$ subtype giving rise to long-range projecting inhibitory neurons, *SST*$^+$/*GUCY1A2*$^+$ contributing to a subset of *SST*$^+$ and *PVALB*$^+$ interneurons likely including the *TH*-expressing subtypes. (**D**) Inhibitory neurons are specified in the subpallium, long before they reach the neocortex (*56*). However, if they are further diversified across the cortical areas is still debated (*32*). AUC scores calculated by Augur representing transcriptomic divergence of inhibitory neurons resulted low (0.682 ± 0.004) for most of the area pairs, indicating limited differences. This result suggests the same inhibitory neuron types are transcriptomically homogenous across cortical areas. However, more prominent divergence were found in the prefrontal areas and IPC. This uniqueness displayed similar patterns in *LHX6* and *NR2F2/SP8* inhibitory neurons lineages, but distinct dynamics between E93 and E110. (**E**) Hierarchical clustering of DEGs across cortical areas in *LHX6* (top) and *NR2F2/SP8* (bottom) cortical inhibitory neurons. The analysis also identified unique expression patterns in the areas of the prefrontal cortex. For each set of DEGs, their expression was visualized in both *LHX6* (left) and *NR2F2/SP8* (right) inhibitory neurons, which exhibited similar expression patterns. (**F**) Correlation of

area expression enrichment between *LHX6* (x axis) and *NR2F2/SP8* (y axis) cortical inhibitory neurons. Here the enrichment is represented by the log fold changes of average expression in a given area versus the background area. The Pearson correlation coefficients were listed on the top left of each panel.

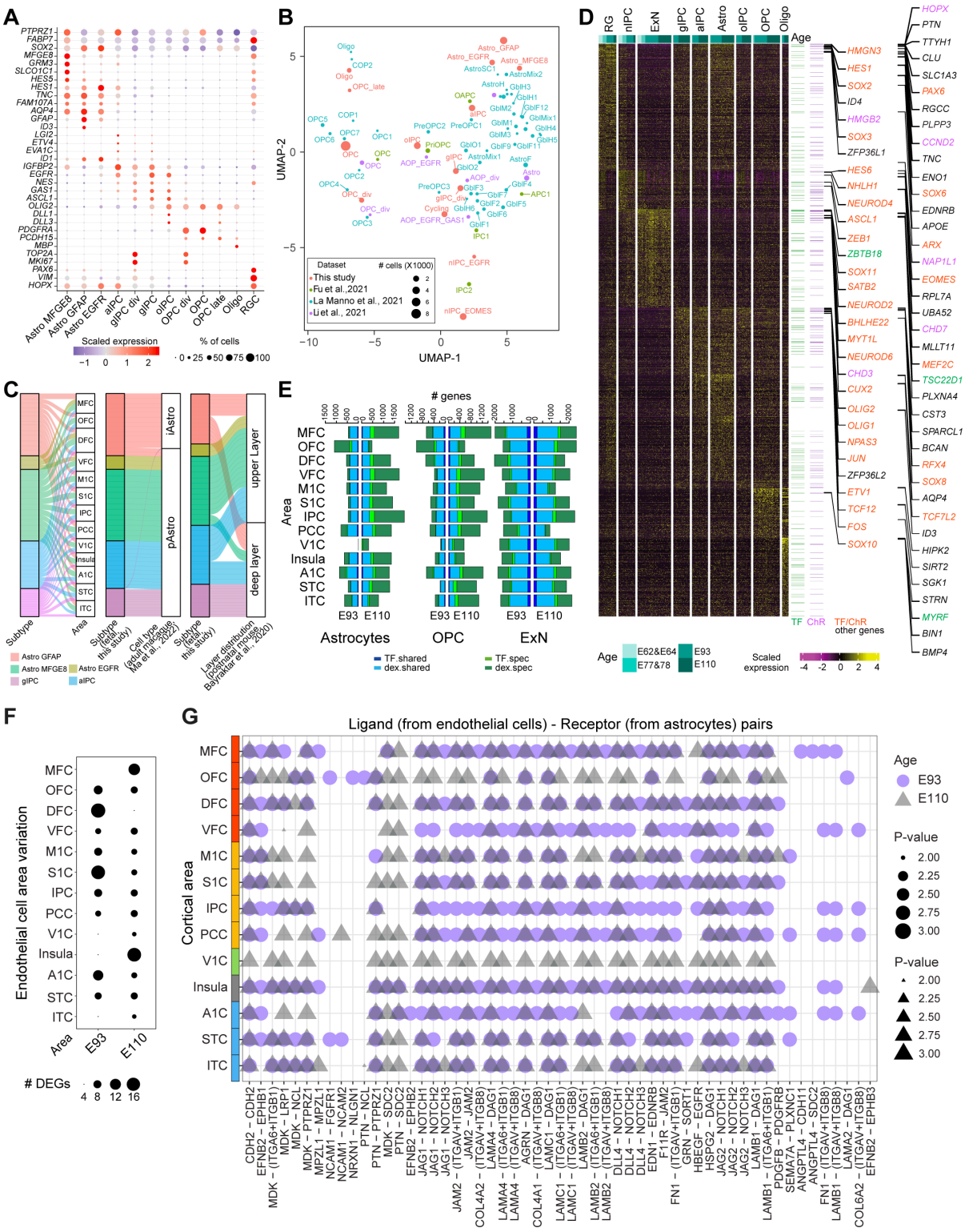

Fig. S15. Cortical arealization during gliogenesis (**A**) Expression of curated genes specific for RG and glia cell subtypes. The color strength and circle size scale the normalized gene expression and the percentages of expressed cells. (**B**) UMAP plot showing data integration of the current study with other

fetal and adult human and mouse datasets (*25, 95, 96*). The circle sizes scale the number of cells identified in each cell type, and the positions represent the geometric centers of the UMAP coordinates of each cell type. (**C**) Alluvial plots showing regional distribution of the astrocyte subtypes defined in this study compared to monkey and mouse adult stage (*30, 72*). We identified three subtypes: one (Astro *EGFR*$^{+}$) enriched in prefrontal regions and the others (Astro *GFAP*$^{+}$ and Astro *MFGE8*$^{+}$) shared across regions. **(D)** Expression of selected genes in radial glia (RG), neuronal IPC (nIPC), excitatory neurons (ExN), glial IPC (gIPC), astrocyte IPC (aIPC), astrocytes (Astro), oligodendrocyte IPC (oIPC), oligodendrocyte precursors (OPC) and oligodendrocytes (Oligo). Transcriptional factors, chromatin modulators and both and other selected genes are highlighted beside the heatmap. (**E**) Bar plots showing the numbers of genes and transcription factors (TFs) identified as differentially expressed across areas in Astro, OPC, and ExN at E93 and E110. Comparisons between E93 and E110 are conducted to reveal the temporal specification of the cells. Notice astrocytes were not detected in V1C at E93 and the data were left empty. TF/dex.shared/spec: number of area-shared or -specific (spec) TFs or differentially expressed genes (dex). **(F)** Dot plots representing the number of genes identified as area-differentially expressed in endothelial cells. (**G**) Astrocyte development is influenced by signaling from endothelial cells (*97*). The figure illustrates predicted interactions between ligand (L) expressed from endothelial cells and receptor (R) expressed from astrocytes for diverse signaling pathways, displaying variation across time (E93 and E110) and cortical areas. Both the circle (E93) and triangle (E110) sizes scale the negative log2 transformed P-values.

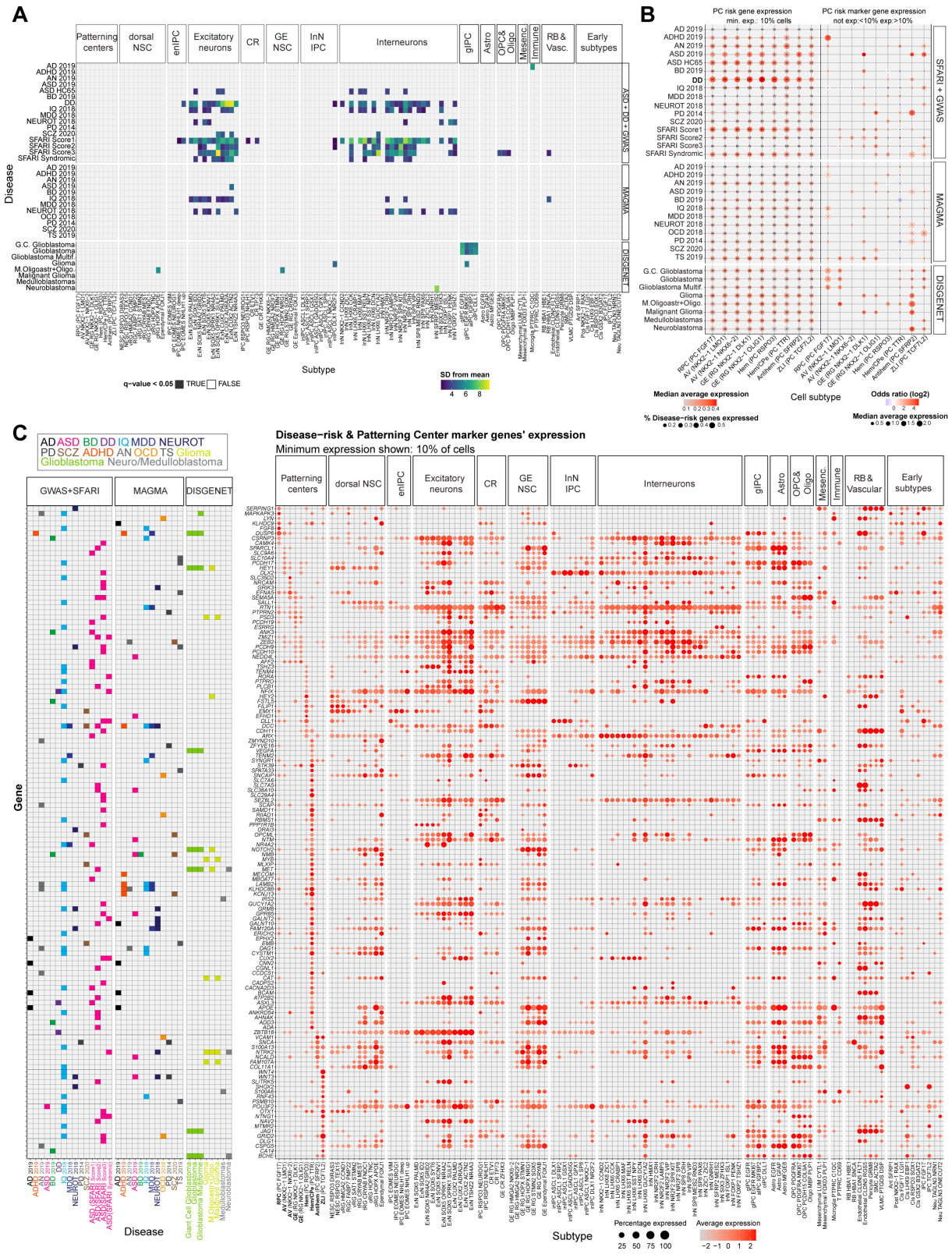

Fig. S16. Expression of brain disease-risk genes in early development (**A**) Heatmap representation of Expression Weighted Celltype Enrichment (EWCE) results. Only significant enrichment results (q-

value < 0.05) are shown. The color scale represents the number of standard deviations over the expected mean of the corresponding enrichment result. Alzheimer's disease (AD), attention-deficit/hyperactivity disorder (ADHD), anorexia nervosa (AN), autistic spectrum disorder (ASD), bipolar disorder (BD), developmental delay (DD), intelligence quotient (IQ), major depressive disorder (MDD), neuroticism (NEUROT), Parkinson's disease (PD), schizophrenia (SCZ), obsessive-compulsive disorder (OCD), Tourette syndrome (TS). (**B**) Left: dot-plot representation of gene expression for disease-associated genes in the organizer domain subtypes. Dot size represents the proportion of disease risk genes expressed in the given subtype. Dot color indicates the median gene average expression of the disease genes. The number inside each dot represents the number of genes from the given disease gene list that are expressed in the subtype. Right: dot-plot summarizing the disease-risk enrichment in organizer domain subtype marker genes. The number inside each dot represents subtype markers overlapping with disease risk genes. The size of each dot represents the median average scaled expression of the overlapping markers. Dot color indicates the odds ratio of a disease risk gene being a subtype marker. **(C)** Scaled gene expression for the 132 markers of organizer subtypes linked to diseases across all the cells. Of these 132 genes, 26 were most distinctive of the organizer domain subtypes and other 106 also appeared later in development in other cells. The marker genes shown are expressed in more than 10% of the cells of an organizer subtype and in less than 10% of in the other organizer cells. In contrast to Fig. 7B, showing 26 gene most distinctive of the organizer domains, filtering was only applied within organizer domain cells, but not other subtypes. The associations between genes and diseases are shown by the panel on the left, by squares colored by disease. Expression <10% of cells in a subtype is not shown. Genes are ordered based on the peak percentage of expressing cells along the organizer subtypes axis and follow alphabetical order (bottom to top). The 106 genes appearing also later in other cells include, for instance, *DUSP6*, associated with ADHD and glioblastomas, known to function in neurons and glia, which here resulted expressed early in the antero-ventral organizer progenitors and later in glial cells. See material and methods for more abbreviations of the diseases.

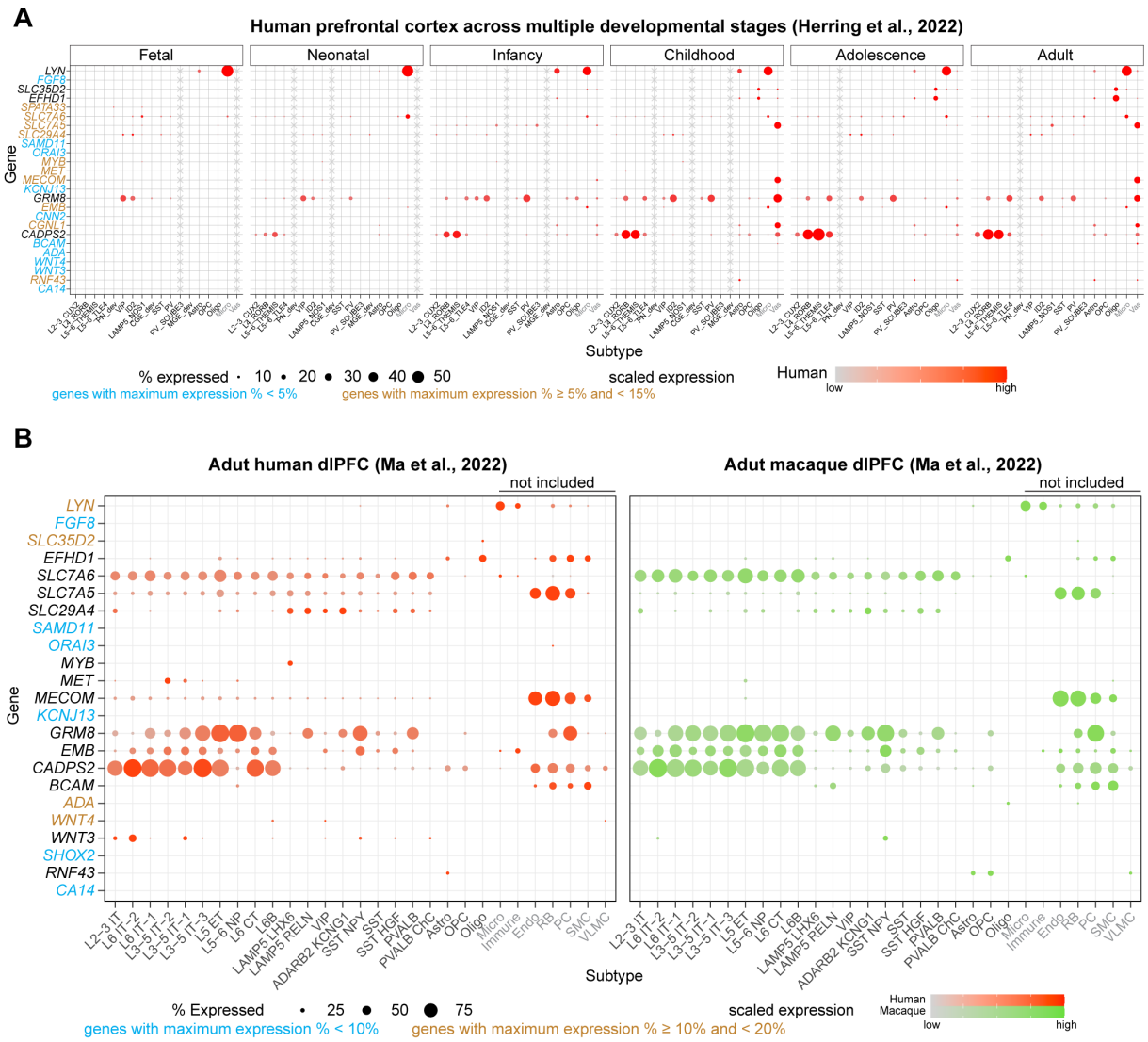

Fig. S17. Expression of brain disease-risk genes across primate lifespan (A-B) The expression of the 26 genes expressed in the patterning centers shown in Fig. 7B was evaluated in multiple snRNA-seq datasets including (A) human prefrontal cortex spanning development from late gestation (GW22 and GW38) to adult stages (*98*) and (B) in another snRNA-seq dataset from adult dorsolateral prefrontal cortex (dlPFC) of humans and macaques (*30*). Because the second snRNA-seq dataset has a relatively higher depth, we set a threshold of 5% for the first dataset and 10% for the second dataset to determine if a gene is expressed or not. Note that *SHOX2* was not found in the Herring et al. dataset, likely because it has low expression and was filtered out. The genes highlighted in light blue or golden indicate no or very low expression in the adult datasets, respectively. Subtypes in light gray in A and B are non-neural cells whose expression of the risk genes was not included in the analysis (materials and methods).

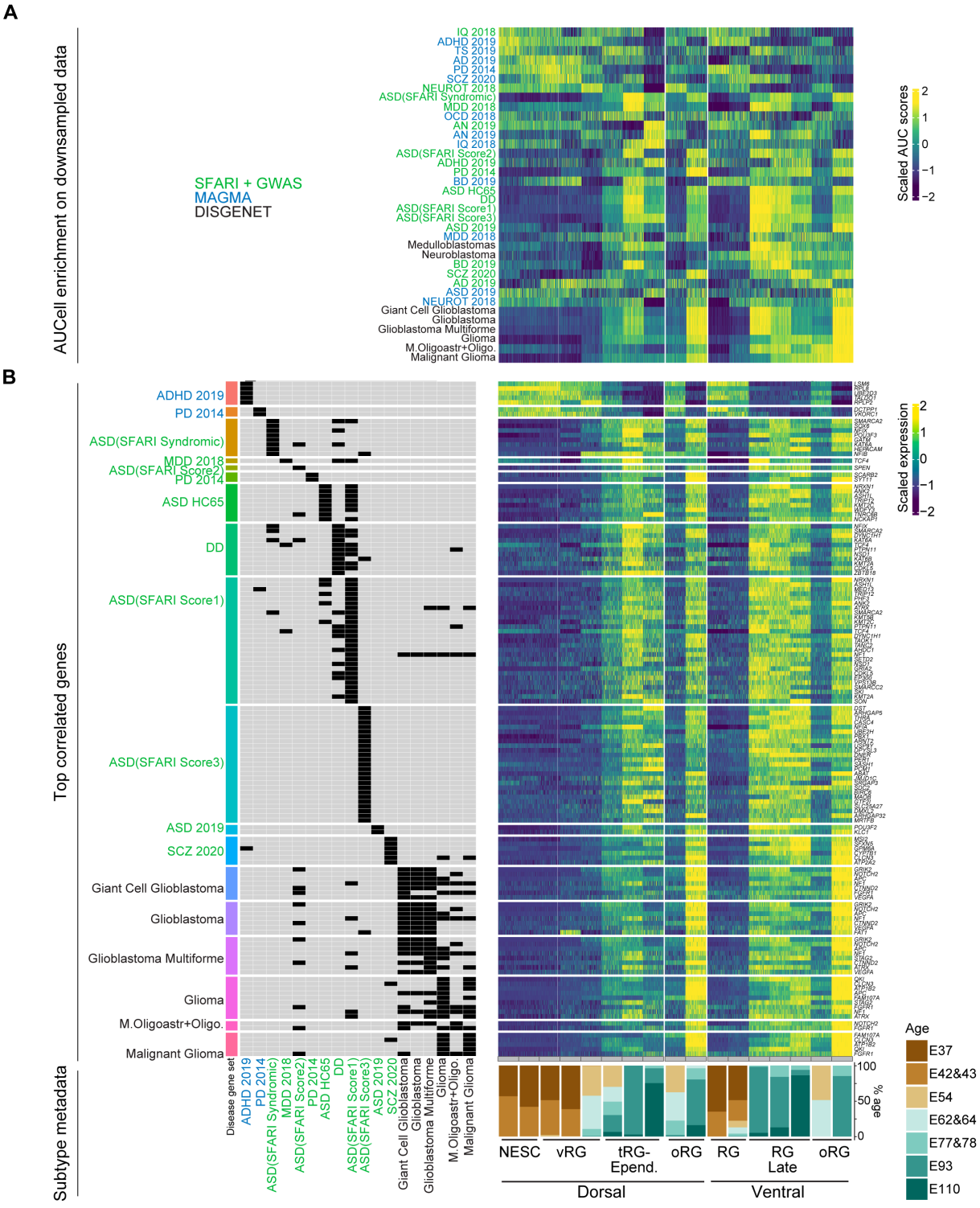

Fig. S18. Enrichment of the disease risk genes along the progression of dorsal and ventral NSCs

(**A**) Scaled AUC scores recapitulating the expression enrichment patterns of the disease genesets across NSC subtypes in the downsampled data. Genesets are arranged in the same order as that in

Fig. 7C. The analysis shows that spatiotemporal enrichment patterns in NSCs is not affected by sequencing depth bias, as demonstrated by the consistent dynamics shown in the downsampled data. (**B**) For each disease geneset, genes highly correlated (Pearson correlation coefficients > 0.7) with the gene set enrichment eigengenes were selected and visualized for expression.

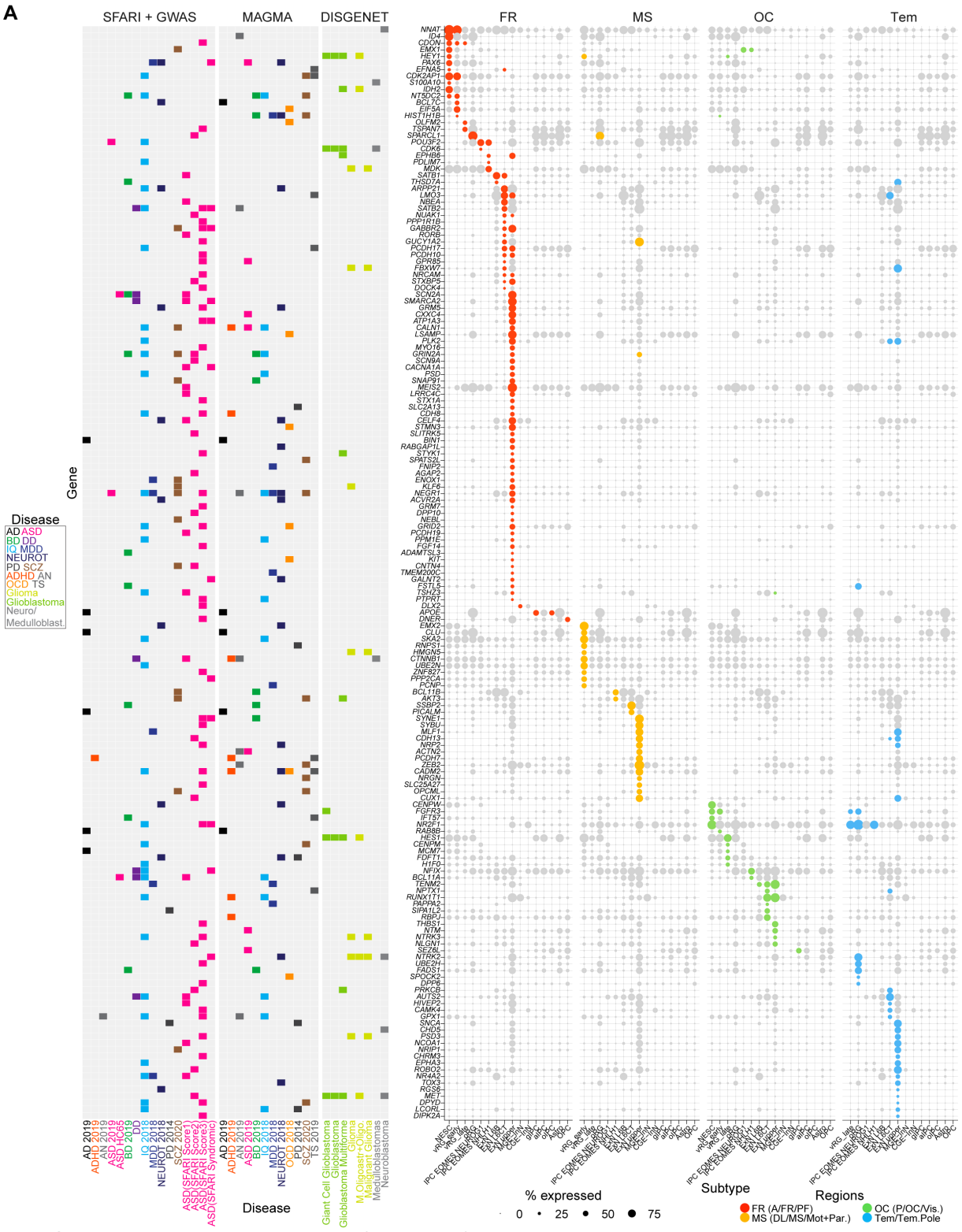

Fig. S19. Regional expression preference of brain disease-risk genes across telencephalic development (**A**) Brain regions might have distinct vulnerability to a disease. For each region/area, all

the disease risk genes showing significant cell subtype enrichment and regional enrichment were selected and visualized. In the dot plot, lightgrey colors refer to no regional enrichment while region colors denote regional enrichment.